Crystal Morphology and Thermodynamics of Poly(ethylene-4,4′-biphenyl dicarboxylate) and Related Copolymers with Ethylene-2,6-naphthalene Dicarboxylate

J. Wendling,[†] A. A. Gusev,[†] U. W. Suter,*[,†] A. Braam,[‡] L. Leemans,[‡] Robert J. Meier,[‡] J. Aerts,[§] J. v. d. Heuvel,[§] and M. Hottenhuis[§]

Department of Materials, ETH, Universitätsstrasse 6, CH-8052 Zürich, Switzerland, DSM Research, NL-6160 MD Geleen, The Netherlands, and Akzo Nobel Central Research, NL-6800 SB Arnhem, The Netherlands

Received December 28, 1998; Revised Manuscript Received July 28, 1999

ABSTRACT: We present a detailed experimental and modeling investigation of poly(ethylene-4,4′-biphenyl dicarboxylate) (PEBB) and the related random copolymers poly(ethylene-4,4′-biphenyldicarboxylate-*co*-2,6-naphthalene dicarboxylate) (PEBB/EN). We find that different polymorphs exist for the PEBB homopolymer and suggest a second crystal unit cell, different from that which is discussed in the literature. PEBB/EN copolymers, which are shown here to be random copolymers, are found to be semicrystalline for all naphthanoate concentrations. By combination of DSC, X-ray, and solid-state NMR experiments, uniform comonomer inclusion is proposed for copolymers containing a high amount of EN; for low EN concentrations, these comonomers are rejected from the crystals. By comparison of the comonomer inclusion Gibbs energy, which was estimated from experiments, to those obtained from thermodynamic integration calculations, it was found that PEBB/EN copolymers are able to cocrystallize by aggregation of like and by segregation of unlike repeat units. Once these comonomer inclusions have reached a considerable size, the average defect Gibbs energy reduces to the thermal energy.

Introduction

The crystallization of random nonflexible main-chain aromatic copolymers[1−5] such as semiaromatic polyesters of the type poly(ethylene terephthalate) (PET), poly(ethylene-2,6-naphthalene dicarboxylate) (PEN), and poly(ethylene-4,4′-biphenyldicarboxylate) (PEBB) (see Figure 1) has up to now not been well understood. The misfit in the crystal created by units of different lengths strongly affects the crystal conformation and crystallization Gibbs energy, because it cannot be "fixed" within a small and localized region of the crystal, especially in the directions of chain extension. In this case, the area of rearrangement influenced by the inclusion can be of the same size as the thickness of the crystal lamellae. For nonaromatic copolymers, e.g., those consisting of units with different length of a flexible side chain (like isotactic poly(propylene-*co*-butene-1), i-PP/B, or poly(*β*-hydroxybutyrate-*co*-*β*-hydroxyvalerate), PHB/HV), the misfit in shape of the co-unit incorporated in the host crystal can be compensated for by small rearrangements of the polymer chains in the surrounding of the defect, without affecting the long-range order of the crystal.

An example of a rigid main-chain aromatic random copolymer is poly(hydroxybenzoic acid-*co*-hydroxynaphthanoic acid).[6] This copolymer does not crystallize but exists in the nematic liquid crystalline state. However, crystallization of these copolymers would be conceivable when the chains arrange by selection of similar and matching, yet random, segments of the chain.[7] The probability of finding those matches is not too small, but it is uncertain whether these aggregates can reach the minimum size of thermodynamically stable nuclei.

[†] ETH Zürich.
[‡] DSM Research.
[§] Akzo Nobel Central Research.

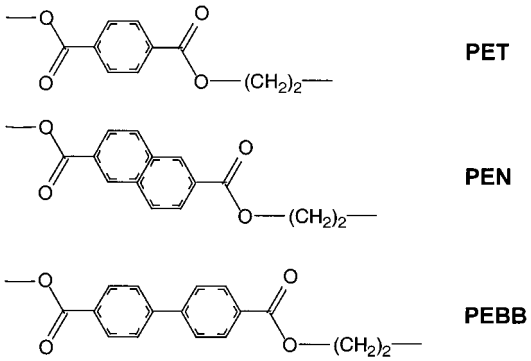

Figure 1. Chemical repeat units of poly(ethylene terephthalate) (PET), poly(ethylenenaphthalene-2,6-dicarboxylate) (PEN) and poly(ethylene-4,4′-biphenyldicarboxylate) (PEBB).

The high molecular rigidity may limit the chain mobility required for constitutional matching of sequences. Increasing the flexibility of these main-chain copolymers might, first, increase the possibility of finding suitable matches; second, more flexible segments in the polymer chain reduce the coupling of the positions of monomers along the chain and enhance the optimization of the conformation toward lower free energy. Semiaromatic polyesters consisting of a rigid aromatic segment and a flexible alkene spacer (Figure 1) are a good example for such semiflexible copolymers. In the literature, a detailed investigation was presented by Lu and Windle[8] for the cocrystallization of random copolymers of ethylene terephthalate (ET) and ethylenenaphthanoate (EN). Isodimorphism was observed with a change of the preferred crystal-lattice type from PET-like to PEN-like at an overall concentration of approximately 30 wt % of ethylene terephthalate in the copolymer. The structure of the crystals was described by nonperiodic layers (NPL) where the units of the same type aggregate in planes perpendicular to the chain orientation.

10.1021/ma982013r CCC: $18.00
Published on Web 10/22/1999

Table 1. Transition Temperatures (DSC) of PEBB and Homologous Compounds from the Literature[a]

no. of aliphatic C atoms	Meurisse et al.[10]		Krigbaum et al.[11]	
	$T_{m,1}$ (K)	$T_{m,2}$ (K)	$T_{m,1}$ (K)	$T_{m,2}$ (K)
2 (PEBB)	587	623		
4	547	566	552	583
6	482	502	452, 482	493

[a] The data of Meurisse et al. are measured applying a heating rate of 20°/min, whereas Krigbaum et al. used a heating rate of 10°/min.

In the present paper, we study EN/EBB copolymers. These systems are interesting for different reasons. Copolymers of ET and EN display lower permeability, film curvature, etc. than PET homopolymers. PEN can be synthesized at low cost, but the melting temperature is relatively high. From copolymerization of EN with EBB, a further enhancement of the gas permeability can be expected, but for processing and applications of those copolymers, it is important to control crystallization and melting temperature.

The PEBB homopolymer has previously been studied by Li and Brisse,[9] Meurisse et al.,[10] and Krigbaum et al.[11] Meurisse et al. measured DSC traces at a heating rate of 20 K/min for a series of semiaromatic bibenzoates: poly(ethylenebibenzoate) (PEBB), poly(butylenebibenzoate), and poly(hexamethylenebibenzoate). The number of carbon atoms in the aliphatic part of the monomeric units are, respectively, 2, 4, and 6. Two transitions are reported: a first transition from the crystal to a mesophase ($T_{m,1}$) and a second transition ($T_{m,2}$) to the isotropic melt. The reported ratios of $\Delta H_m^1/\Delta H_m^2$ vary from ca. 0.15 to 1.5 for C2 to C6. The melting temperatures are summarized in Table 1.

Krigbaum reported similar results for the same materials from DSC experiments with a heating rate of 10 K/min. From the compound containing two aliphatic C atoms per monomeric unit, no melt peaks could be detected, in contrast to compounds containing four and six aliphatic C atoms. The results are also summarized in Table 1. Except for PEBB (two C atoms) the results of Meurisse and Krigbaum largely agree. According to Li and Brisse who based their interpretation on the results reported in refs 10 and 11 but extracted equilibrium transition temperatures, the melting of PEBB occurs in two stages. At 610 K, the crystal structure is transformed into a mesophase, and at 640 K, an isotropic melt is formed. Li and Brisse also described the crystal structure of PEBB.[9] They found that the X-ray pattern could be indexed as either monoclinic or triclinic, but from density measurements only the triclinic unit cell ($P\bar{1}$ symmetry) remained possible. The reported unit cell parameters are as follows: $a = 5.73$ Å, $b = 3.77$ Å, $c = 14.73$ Å, $\alpha = 89.8°$, $\beta = 89.8°$, and $\gamma = 79.0°$.

In the first part of this paper, we present an experimental investigation of the PEBB homopolymer and PEBB/EN copolymers at hand together with a computational investigation of the crystal structures. In the second part, we present calculations of the defect Gibbs energy of PEBB/EN copolymer crystals with various concentrations and states of ordering of the comonomers, leading to an estimate of the melting temperature based on computational methods described previously.[12]

Experimental Details

One may doubt whether the solubility of the PEBB polymer is sufficiently high, during synthesis, such that it remains dissolved, thereby allowing it to reach a reasonable molecular weight. Therefore, two independent polymerization trials have been done. The polymerization of PEBB **1** was done as described in ref 13: a 250 mL three necked round-bottom flask was filled with 3.88 g of glycol (0.0625 mol), 17.45 g of 4,4′-bibenzoyl chloride (0.0625 mol), and 150 g of α-chloronaphthalene. This mixture was heated to 220 °C. At a temperature of 125 °C, the mixture became clear, but a few minutes later, at a temperature of 150 °C, the solution became hazy again, probably due to crystallization of the polymer. After 24 h of stirring at 220 °C, the white cloudy solution was cooled to room temperature. No obvious increase in viscosity was observed. The suspension was coagulated in methanol, filtered, washed with methanol, and dried. A fine, almost white powder was obtained.

The polymerization of PEBB **2** was accomplished according to work of Qing et al.:[14] a 400 mL cylindrically class autoclave reactor was filled with 3.10 g of glycol (0.050 mol), 13.96 g of 4,4′-bibenzoyl chloride (0.050 mol), and 200 g of 1,1,2,2-tetrachloroethane. This mixture was heated, while stirring, to 70 °C. Then, the mixture became clear and 15.82 g (0.20 mol) of pyridine was added. Then the temperature was rapidly raised to 90 °C, and the solution became hazy. Subsequently, the temperature was raised to reflux temperature (145 °C), and the white cloudy solution was stirred for another 4 h. During the reflux period, the white solution turned slowly yellow and finally to a dark green cloudy suspension. After 4 h of reflux the suspension was cooled to room temperature. At room temperature the dispersion showed some viscosity. The suspension was coagulated in methanol, and after filtration, extensive washing with methanol, and drying, a fine, slightly colored powder was obtained.

The polycondensation of PEBB/EN copolymers was performed in a glass autoclave using a standard PEN procedure. Starting materials are dimethyl-2,6-naphthalene dicarboxylate, glycol, and dimethyl-4,4′-biphenylene dicarboxylate. $Mn(OAc)_2 \cdot H_2O$ (2.5% solution), a phosphorus stabilizer, and a Sb_2O_3-based solution were consecutively used as catalysts. The methanol distillation started at ca. 175 °C. After distillation of the methanol, at ca. 215 °C product temperature the excess glycol was distilled off. At approximately 245 °C the phosphorus stabilizer was added, and at approximately 250 °C (minimal 5 min later) the Sb_2O_3 solution was added. At a product temperature of 260 °C, polycondensation started. A 100 mbar vacuum was drawn by a water-jet-pump; thereafter, an oil pump was used for obtaining deep vacuum (<1 mbar). After about 1 h at a product temperature of 290 °C, the polymerization was stopped and the polymer melt was extruded into a water bath. The cooled strands were cut into granules and dried at 105 °C under vacuum, overnight.

For differential scanning calorimetry and X-ray analysis, all samples were dried at 130 °C for 24 h in a vacuum oven with a slight nitrogen purge. Dried samples were pressed to plates with a pressure of approximately 15 kN at temperatures in the range 200−250 °C, depending on the composition. Parts of these samples were once more annealed at 200 °C for at least 24 h in a vacuum oven with a nitrogen purge.

DSC experiments were performed on a Perkin-Elmer DSC 7 using nitrogen as a purge gas. The heating rate was 10 °C/min. Wide-angle X-ray diffraction measurements were performed using either of two powder diffractometers in Bragg−Brentano geometry: a Philips PW1820 for measurements under helium atmosphere and a Philips PW1050 for data collection under ambient conditions. All experiments used Cu Kα radiation, a monochromator in the diffracted beam, a discrimination level of 35−70%, a divergency slit of 1°, a receiving slit of 0.2 mm, and a scatter slit of 1°. Diffraction patterns were measured with a resolution of $\Delta 2\theta = 0.05°$ and a counting time of 10 s. The spacings have been corrected for sample transparency according to Wilson,[15] based on a linear absorption coefficient, μ, of 8 cm^{-1} and a thickness of 2 mm for all samples. Small-angle X-ray diffraction measurements were performed with a Kratky camera under ambient conditions, using nickel-filtered Cu Kα radiation and a position sensitive detector. The patterns were corrected for instrumen-

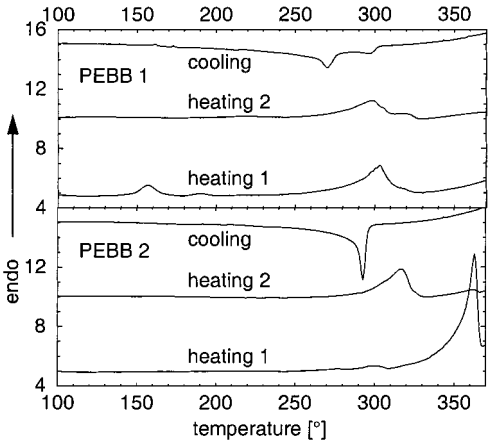

Figure 2. DSC traces of PEBB **1** and **2**, measured with a heating (cooling) rate of 10 K/min.

Table 2. DSC Results of Our PEBB Samples 1 and 2

polymer	T_m(first heating) (K)	T_m (second heating) (K)	ΔH_m(second heating) (J/g)
PEBB **1**	576	571	40.1
PEBB **2**	636	590	40.4

tal scattering using the scattering pattern of the empty camera and the transmission coefficient of the sample. Absolute intensities were obtained using a Marlex standard.

^{1}H NMR spectra were recorded in solution at 363 K, at the KU Nijmegen on a AM-500 spectrometer with a ^{13}C-measuring frequency of 125 MHz. The samples were first cut into small pieces and subsequently dissolved in *p*-cresol, approximately 30 mg/0.5 mL for the 5 mm dual probe. A power-gated decoupling was used, and more than 10 000 scans had to be accumulated to obtain an acceptable signal-to-noise ratio. The relaxation time was approximately 5 s. A capillary with DMSO-d_6 was added for locking. Regarding data manipulation, no resolution enhancement was applied.

Solid state ^{13}C NMR experiments were carried out on a Varian Unity 400 spectrometer using a 7 mm VT CP/MAS probe. All spectra were recorded under magic angle spinning (MAS) conditions and high-power proton decoupling. The spinning rate was 6 kHz. The 90° pulse on protons and carbons was 5 μs, the recycle delay 10 s. The cross-polarization time was 3 ms. ^{13}C $T_{1\rho}$ relaxation experiments were performed to monitor the local mobility of the individual carbons of PEN and PEBB. The samples were annealed at 200 °C for 2 h and subsequently cooled to room temperature at a low rate (1 °C/min), to obtain the highest possible crystallinity. The NMR relaxation experiments were performed at 130 °C (above T_g of PEBB/EN) in order to achieve a better discrimination between the mobility of the amorphous and crystalline phase.

Analysis of the PEBB Homopolymer

DSC Investigations. The heating curves of our two PEBB samples (**1** and **2**) are shown in Figure 2. The characteristics are presented in Table 2. For sample **1**, only one first-order transition is determined (for the first heating as well as for the second). Referring to the interpretation of Li and Brisse,[9] $T_{m,1}$ is measured, whereas $T_{m,2}$, the transition from a mesophase to the melt, could not be detected. The same result was found for the second heating curve of **2**. However, in the first heating curve of **2** only $T_{m,2}$ is observed, which is also in contrast to the data of Meurisse[10] who detected a large transition peak at $T_{m,1}$.

X-ray Investigations. X-ray powder pattern of PEBB **1** and **2** are presented in Figure 3, and lattice spacings are summarized in Table 3, together with the fiber diffraction data from Li and Brisse. From a comparison

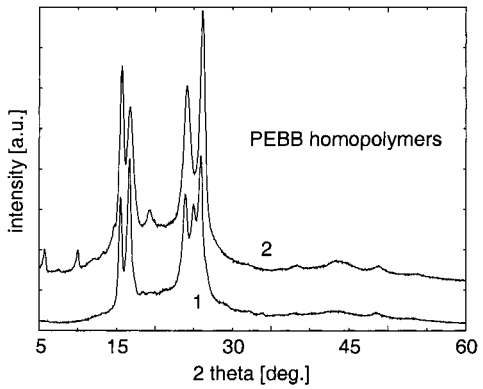

Figure 3. X-ray powder pattern of virgin PEBB **1** and **2**.

Table 3. Experimental Spacings (in Å) for PEBB, Taken from the Literature, Compared to Those of PEBB 1 and 2[a]

hkl	fiber diffraction[9]	PEBB **1**	PEBB **2**
001			14.77
			11.38
002	7.364		8.71
			6.536, 5.940
$\bar{1}00$	5.628	5.612 (44)	5.545
$\bar{1}01$, 101	5.252, 5.263 (5.257)	5.235 (44)	5.206
$\bar{1}02$	4.465		4.527
010, $\bar{1}03$, 004	3.699, 3.694, 3.682 (3.696)	3.686 (24)	3.651
110	3.404	3.407 (36)	3.377

[a] Some spacings from fiber diffraction are averaged as peak overlap may occur. Data for PEBB 1 include an estimate of the experimental uncertainty of the last two digits.

of the data of Li and Brisse and PEBB **1**, it is concluded that the lattice spacings of both samples are identical within experimental error. The (011), ($0\bar{1}1$) reflection that also occurs in Figure 3 is not included in the analysis; this reflection overlaps with the (110) reflection, leading to a shift in peak position.

For PEBB **2**, the observed lattice spacings indicate the presence of a crystal lattice different from the single-crystal lattice data reported by Li and Brisse. The absence of the (011) and ($0\bar{1}1$) reflections in the present powder pattern (although clearly present for PEBB **1**) and the observation of a lattice spacing of 8.71 Å which differs too much from the single-crystal spacing to attribute to experimental inaccuracy, leads to the conclusion that PEBB exhibits polymorphism.

Combining DSC and X-ray data leads to the following conclusions: PEBB **1** contains crystals with the crystal structure as described by Li and Brisse. At approximately 580 K, a transition is observed, most probably the transition from a crystal phase into a mesophase. The transition into an isotropic melt is not observed. PEBB **2** exhibits a crystal structure different from that of PEBB **1** (and as yet unknown). However, crystallization from the melt favors the formation of the same crystal phase. These results suggest that a strong tendency toward polymorphism exists for the PEBB polymer. This might be due to the existence of different conformations with similar crystallization Gibbs energy, when the polymer can crystallize differently by the influence of intrinsic parameters such as the degree of polymerization etc. The existence of such various conformations of similar energy was found by one of us in calculations on PET and other polymers.[16] We now present the investigation of the PEBB crystal structure based on force-field molecular dynamics calculations.

Table 4. Experimental and Calculated Unit Cell Parameters for PET, PEN, and PEBB[a]

	PET		PEN		PEBB		
						simltd	
param	ref 17	simltd	ref 18	simltd	ref 9	1 chain	2 chains
a (Å)	4.5	4.69	6.51	6.50	5.75	5.62	5.78
b (Å)	5.9	5.98	5.75	5.78	3.82	3.97	7.44
c (Å)	10.76	10.96	13.2	13.38	14.62	15.33	15.02
α (deg)	100.3	101.2	81.2	83.4	90.1	70.5	90.1
β (deg)	118.6	121.9	144.0	144.4	90.3	92.4	90.1
γ (deg)	110.8	110.5	100.0	98.4	78.1	81.1	80.3

[a]The calculated data were obtained by averaging over 50 ps MD runs on a crystal microstructure at 300 K. Key: param, parameter; simltd, simulated.

Computational Analysis of the PEBB Crystal Structure. The crystal unit cell parameters of PET, PEN and PEBB have been reported in the literature.[13,17,18] We found that (among others) the PCFF91 force field[19,20] was capable of modeling the unit cells of PET and PEN with high accuracy, (see Table 4) but we were not able to reproduce the triclinic PEBB unit cell as described by Li and Brisse[9] as stable structures with any force field we tested; also changes in the treatment of the nonbonded energy calculation (different cutoff distances or the calculation of the Coulomb energy via Ewald sums) did not succeed. However, some indications were given in the original literature of Li and Brisse[9] that the unit cell of PEBB may be not triclinic but monoclinic. The monoclinic unit cell had been discarded because the experimental data gave no evidence that the unit cell would contain two polymer chains.

To enable modeling of PEBB crystal structures, we searched for an alternative crystal unit cell that is reasonable from the molecular arrangements and that would show agreement with the experimental X-ray pattern of Li and Brisse. Their proposed triclinic unit cell contains only one repeat unit; as the cell angles α and β are close to 90°, the aromatic rings are all in a face-to-face arrangement. However, this is not true for the PET and PEN crystal structures, where the aromatic rings are facing carbonyl units, and it is also not true for the diethyl 4,4′-biphenyldicarboxylate that was used by Li and Brisse as a model compound.[9] The angle β changes from 118.6° for PET to 144° for PEN. For PEBB, the crystal unit cell in the original literature is indexed differently, the corresponding angle being α (and γ of PEBB is identical to 180° − γ of PET and PEN). In MD calculations, we found a stable conformation for $\alpha = 70.54°$ and $b = 3.97$ Å; however, calculated X-ray patterns based on these unit cell parameters are not consistent with the experimental data.

Another stable structure was found with $\alpha \approx 28°$ and $b \approx 8.3$ Å; this is similar to a monoclinic unit cell containing two chains (the unit cell parameters are given in the last column of Table 4). The second chain is shifted by half of the unit cell *c*-axis length and, to increase the similarity to the experimental X-ray pattern, turned by 180° around its long axis. Compared to the cell parameters proposed by Li and Brisse, only *b* is doubled. Figure 4 displays a sketch of both our suggested unit cell and that of Li and Brisse. The average cell parameters taken from the 50 ps MD runs listed in Table 4 are close to those obtained experimentally (except that the *b* axis is now twice as long) and emphasize that this crystalline packing might be a good representation of melt-crystallized PEBB. The effects

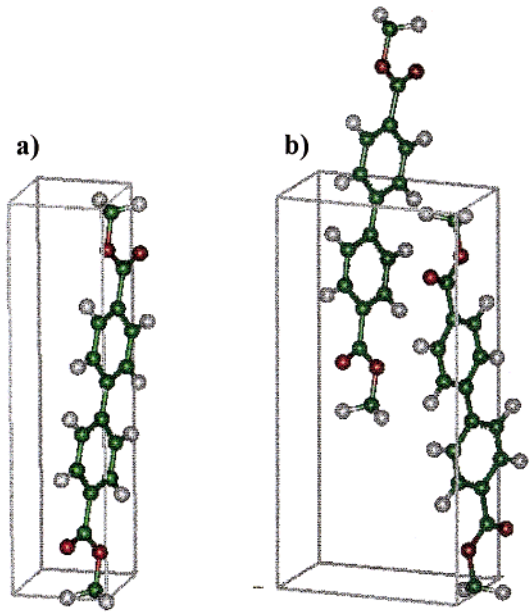

Figure 4. (a) Sketch of the experimentally observed PEBB unit cell. (b) Sketch of the PEB unit cell that was used for molecular dynamics calculations.

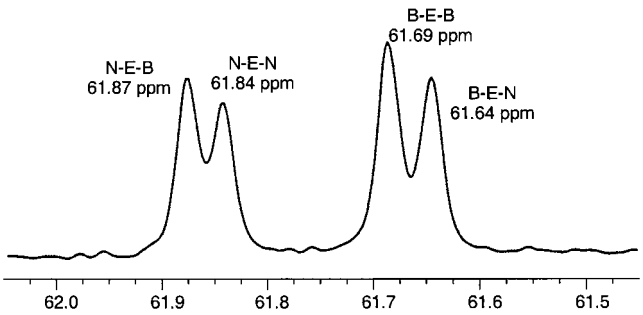

Figure 5. ^{13}C spectrum of PEBB/EN sample, with assignments indicated.

on the X-ray pattern are expected to be very small. Patterns calculated based on the triclinic and monoclinic unit cell were found to differ only in weak spots that may not be observable in our experiment.

Although the new unit cell, constructed with the aid of atomistic simulation, appears to be as realistic as that constructed by Li and Brisse, we have no proof that our guess is the better one. Nevertheless, the fact that a structure exists, different from that of Li and Brisse, that seems to be of comparable stability leads us again to the conclusion that several crystal packings and therefore polymorphism are conceivable for PEBB.

PEBB/EN Copolymers

Sequencing of Copolymers. It is often assumed that copolyesters are random copolymers. This, however, has only been verified experimentally in relatively few cases. To understand the cocrystallization of PEBB/EN copolymers, we investigated the randomness of the copolymers explicitly. This was accomplished through NMR measurements. The ^{13}C spectrum of the homopolymer PEN showed a single peak at about 61.85 ppm. All PEBB/EN samples comprised four peaks, except for samples with very low EBB content.

The interpretation of the NMR spectra is indicated in Figure 5. The two carbon atoms in the ethylene unit joining the aromatic units exhibit an NMR shift which depends on the neighboring aromatic system. When

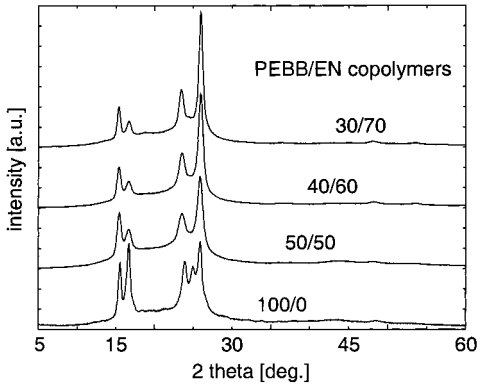

Figure 6. X-ray powder pattern for PEBB, PEN, and PEBB/EN copolymers.

Table 5. Calculated and Experimental Intensity Fractions of the NMR Peaks Due to (left to right) N−E−N, N−E−BB, BB−E−N. and BB−E−BB Sequences, Where N Represents a Naphthanoate Unit, BB a Bibenzoate Unit, and E an Ethylene Bridge

	relative intensities	
composition EBB/EN	from experiment	assuming randomness
0/100	100:0:0:0	100:0:0:0
5/95	94:3:3:0	90:5:5:0
10/90	83:8:9:0	81:9:9:1
15/85	72:12:13:3	72:13:13:2
20/80	65:14:15:5	64:16:16:4
30/70	50:21:22:7	49:21:21:9

both ethylene carbons have the same neighboring aromatic system, either an N or a BB, they exhibit the same NMR shift. This shift is higher (61.84 ppm) when both neighbors are N and is 61.69 pm when both neighbors are BB. When one neighbor is N and the other is BB, the two carbon atoms in the ethylene unit exhibit different shifts: 61.87 ppm for the carbon closest to N and 61.64 ppm for the carbon closest to BB.

The four peaks in the experimental spectra were fitted using fixed peak positions, fixed line shape (Gauss−Lorenz), and fixed peak width. The relative intensities, expressed as percentages of the total intensity for each sample, have been collected in Table 5. If the copolymers were extremely blocky, there would be no peaks due to N−E−BB and BB−E−N. We do observe such peaks, however. For completely random copolymers, we may calculate the expected ratio of the ^{13}C peaks straightforwardly as the values presented in the third column of Table 5. By comparing these calculated data and the experimental numbers, we have to conclude that, within the limits of experimental accuracy, these copolymers are of entirely random constitution.

Wide-Angle X-ray Investigations. X-ray powder patterns (Figure 6) show crystallinity for all EN concentrations and look very similar for PEBB and PEBB/EN copolymers. Only broadening occurs for some of the peaks and the 011 and $0\bar{1}1$ peaks are absent for the copoymers. The disappearance of these peaks is consistent with a reduced three-dimensional long-range ordering of the crystal that occurs when units of different length (in the *c* direction, but similar shape of the *a*−*b* protection, crystallize or when the crystal size decreases. The peak positions reported in Table 6 indicate no significant variation in the copolymers up to an EN composition of 70%; the variations are within experimental errors.

Table 6. Experimentally Obtained Lattice Spacings (in Å)[a]

hkl	PEBB **1**	50% EN	60% EN	70% EN
$\bar{1}00$	5.61(4)	5.75(5)	5.76(3)	5.80(3)
$\bar{1}01$	5.24(4)	5.34(3)	5.34(3)	5.36(4)
010	3.686(24)	3.795(13)	3.792(32)	3.832(30)
110	3.407(36)	3.449(09)	3.444(24)	3.462(24)

[a] PEBB **1**: homopolymer. 50%−70% EN: PEBB/EN random copolymers. The errors are estimated from multiple measurements using different experimental conditions.

At first blush, it would seem that identical diffraction patterns indicate identical crystal units, i.e., that up to 70% EN only the PEBB segments crystallize (comonomer exclusion crystallization). For that case one would expect a strong decrease of the crystallinity even at low comonomer concentrations and an amorphous regime at intermediate composition. This is obviously not the case for the copolymers at hand. For the contrary case of comonomer inclusion one might expect a systematic variation of the crystal spacings as it was also found by Lu and Windle[8] in fiber patterns of PET/EN copolymers. In our powder measurements, the 001 reflections are not directly observed and the 101 reflection, which remains almost unchanged, is not related to the crystallographic repeat unit length only; this makes the estimation of the crystal composition from the X-ray powder pattern impossible. We calculated the pattern from atomistic models to ensure that the experimental powder pattern can be from copolymer crystals.

Simulation of the X-ray Powder Pattern. PEBB-based crystals comprising random comonomers (EN inclusions in PEBB crystals) were built to investigate more realistic cocrystal structures. The procedure was as follows: first, on a lattice of $6 \times 4 \times 6$ constitutional repeating unit sites, representing a PEBB crystal microstructure consisting of 24 stems with 6 repeat units each, one (or two, or three, for higher EN concentrations) randomly selected lattice site(s) of each stem was replaced by the EN unit. The incorporation of an equal number of units in all stems does not conform to random comonomer inclusion, but it ensures that all stems have the same length after transformation of the lattice model into an atomistic model, reducing constraints related to the finite size of the model. In a second step, the stems were individually shifted along their long axis to lower the total energy of the lattice. The Hamiltonian used for this optimization is coarse-grained and comprises longer stems with random comonomer sequences, which will be discussed below. Here it suffices to say that this Hamiltonian favors the aggregation of repeat units of the same type into layers in the *a*−*b* plane of the crystal microstructure. Because of the random nature of the copolymers, no total segregation into layers can occur; instead, we observe segregation into an EN-rich region (an "incomplete layer"), surrounded by an EBB-rich zone, and a remaining, random region. The initially random and the optimized lattice structures were translated into atomistic microstructure models suitable for force-field calculations and minimized with respect to the (atomistic) potential energy after a short relaxation via a molecular dynamics run. An example on the effect of the optimization procedure is given in Figure 7. EBB units are labeled in dark gray, EN units are labeled in light gray. Whereas the initial structure appears to be completely random, EN-rich and EBB-rich layers are formed during optimization. From sets of 10 so-obtained microstructures each with con-

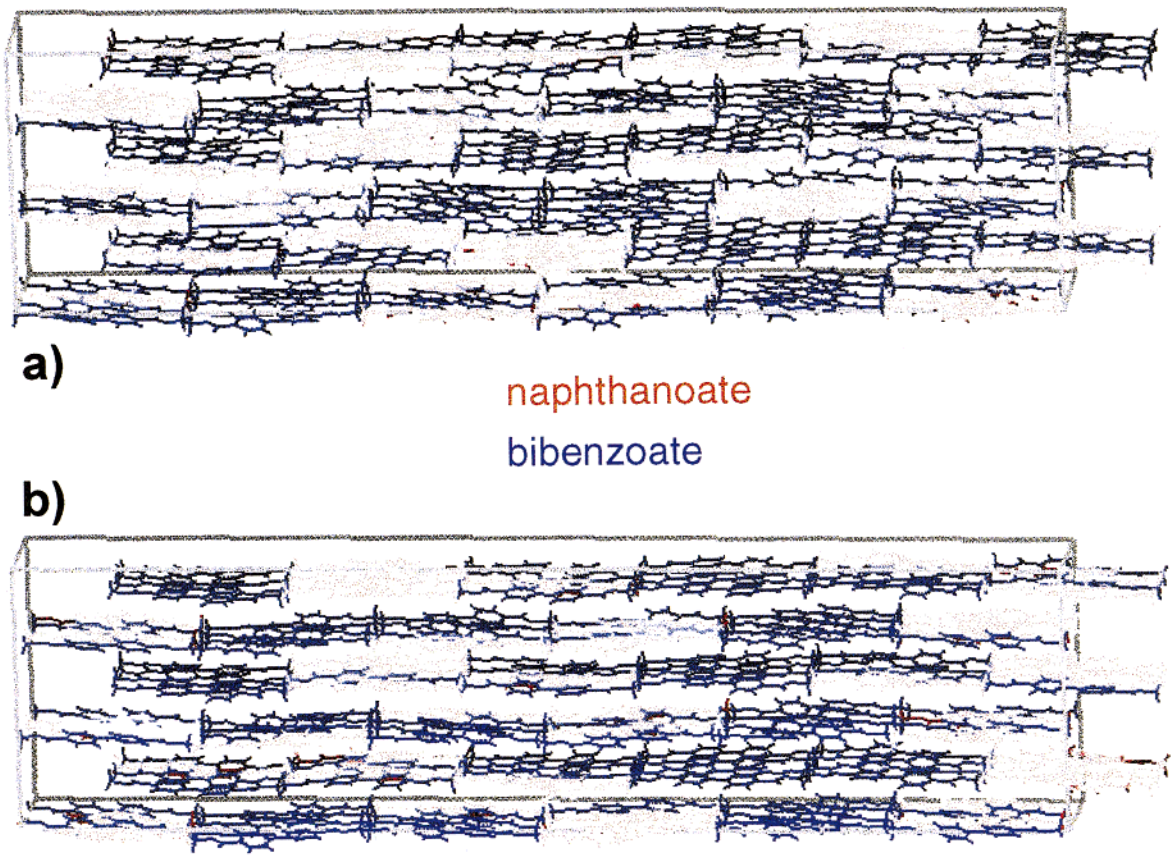

Figure 7. (a) Random PEBB/EN cocrystal (33.3% naphthanoate). (b) Same structure after "optimization" on a lattice. Bibenzoate units are shown in blue, whereas naphthanoate units are shown in red.

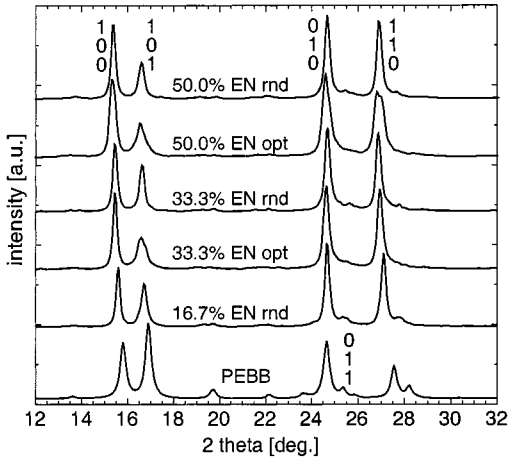

Figure 8. Average of all X-ray patterns calculated for the same naphthanoate concentration and the same state of optimization. PEBB: homopolymer microstructure; copo 16.7%. EN rnd (33.3% EN rnd, 50% EN rnd): one (two, three) EN in each chain at random selected position; copo 33.3%. EN opt (50% EN opt): two (three) EN in each chain at random position after optimization on a lattice and force-field energy optimization.

centrations of EN units of 16.7%, 33.3%, and 50%, the X-ray powder patterns are calculated.

All X-ray patterns calculated for a set of microstructures with the same EN concentration and state of optimization are very similar in lattice spacings and structure factor. Average patterns for each concentration and conformation are shown in Figure 8. They show minor differences only, although the composition and randomness of the microstructures have changed. Lattice spacings calculated from these simulated peak positions are reported in Table 7.

Table 7. Calculated Lattice Spacing for Different Copolymer Compositions and Different States of Optimization[a]

hkl	100% PEBB	16.6% EN random	33.3% EN optimized	33.3% EN random	50.0% EN optimized	50.0% EN random
100	5.60	5.69	5.73	5.75	5.77	5.76
$\bar{1}01$	5.24	5.30	5.34	5.34	5.35	5.34
010	3.609	3.609	3.609	3.602	3.616	3.609
$0\bar{1}1$	3.511	3.490	3.490	3.47		3.504
110	3.241	3.288	3.306	3.311	3.324	3.318

[a] Random: microstructure as obtained after random fill. Optimized: microstructure as obtained after optimization on a lattice.

Comparing these simulated results and taking account of the experimental X-ray patterns, we conclude that the observation that the latter patterns look very similar for different overall comonomer compositions gives no support to the assumption that the crystals are made up by EBB segments only. Uniform inclusion of EN units is possible as is total exclusion, and the real EN concentration must be obtained from other experiments. One possible such experiment is solid state NMR, for which we subsequently selected the 30/70 (EBB/EN) copolymer to investigate the crystal composition.

Solid State NMR. In Figure 9 the ^{13}C spectra of the homopolymers PEN and PEBB and of PEBB/EN with 70% EN are plotted. The resonances of three different types of carbons are visible: carbonyl carbons (~165 ppm), aromatic carbons (~130 ppm), and the aliphatic carbons of the ethylene glycol unit (~65 ppm). Because

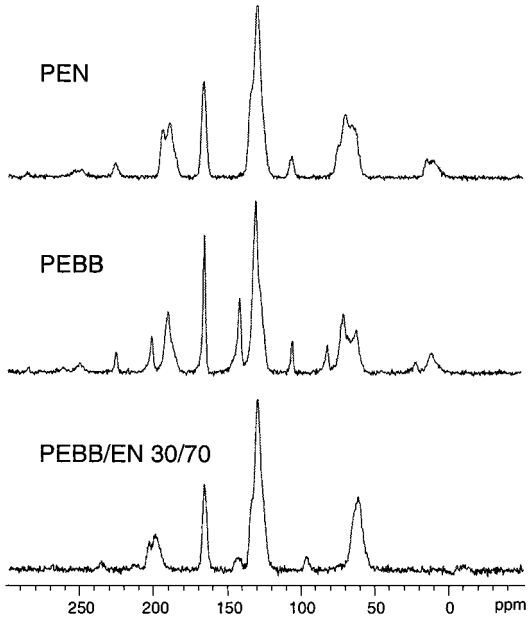

Figure 9. ^{13}C CP−MAS solid-state NMR spectra of PEN (A), PEBB (B), and 30/70 PEBB/EN copolymer (C).

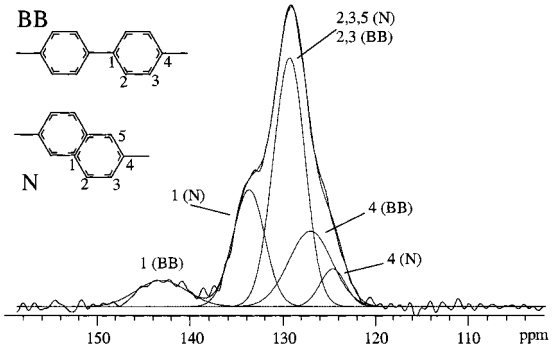

Figure 10. Deconvoluted ^{13}C CP−MAS spectrum of a 30/70 PEBB/EN copolymer showing the aromatic resonances.

of the rigidity of these polymers and the large chemical shift anisotropy, intense spinning sidebands of the carbonyl and aromatic carbons are visible (marked with an asterisk). The carbonyl and aliphatic resonances of the EN and EBB constitutional repeating units overlap strongly. Only the resonances of the aromatic carbons of BB and N are partly resolved. This is shown more clearly in a spectrum of the aromatic region, shown in Figure 10, where an attempt was made to decompose the broad bands into individual peaks. The assignments as indicated in the figure are based on the ^{13}C spectra of the pure components and on solution spectra.

By performing ^{13}C $T_{1\rho}$ experiments, the mobility of individual carbons can be observed. The NMR relaxation decays are sensitive to molecular motions in the midkilohertz frequency regime. Using spectral deconvolution of the aromatic region, the relaxation decay of the aromatic carbons of the BB and N moieties could be determined. These relaxation decays are shown in Figure 11; all were clearly not monoexponential but could be interpreted with biexponential decays. The solid curves represent least-squares fits to the experimental data using a two-exponential function. From these fits, the relaxation time constants ($T_{1\rho}$(A), $T_{1\rho}$(B)) and their corresponding fractions (I(A), I(B)) could be determined.

Obviously, for all carbons a relaxation decay is observed which is composed of two components: a fast

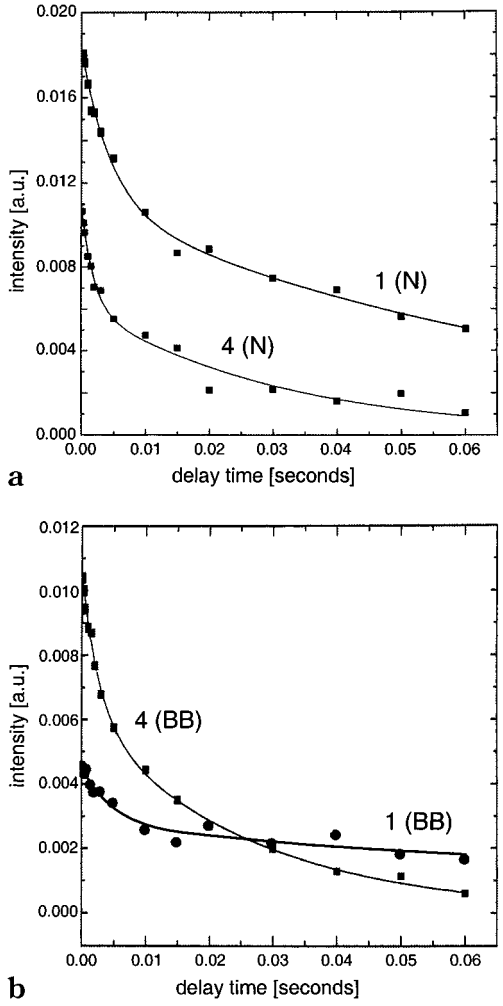

Figure 11. ^{13}C $T_{1\rho}$ relaxation decay of nuclei of a 30/70 PEBB/EN copolymer.

Table 8. ^{13}C $T_{1\rho}$ Relaxation Time Constants and Fractions of the Individual Carbons

type of carbon	$T_{1\rho}$(A) (ms)	I(A)	$T_{1\rho}$ (B) (ms)	I(B)
1 (PEBB)	4.5 ± 1.6	0.43 ± 0.07	135 ± 61	0.57 ± 0.07
4 (PEBB)	2.7 ± 0.4	0.42 ± 0.04	26 ± 2	0.58 ± 0.04
1 (PEN)	4.6 ± 0.7	0.40 ± 0.03	80 ± 10	0.60 ± 0.03
4 (PEN)	1.9 ± 0.6	0.44 ± 0.06	32 ± 5	0.56 ± 0.06

relaxing component (A) in the range of 1.9−4.5 ms (about 40% of total decay) and a slow relaxing component (B) in the range of 26−135 ms (about 60% of total decay). These data are listed in Table 8. Although it is known that aromatic carbons may show a complex nonmonoexponential NMR relaxation decay, it is likely that the slow relaxing component is due to carbons with restricted mobility in the crystalline phase and the faster relaxing component to carbons in the more mobile amorphous phase. Since this two-component relaxation behavior is observed both for EN and EBB units, this indicates that both monomer types are incorporated into the crystals. Even more, since the fractions of "rigid" (∼60%) and "mobile" (∼40%) material is comparable for naphthanoate and bibenzoate, it is proposed that for this particular copolymer the crystalline phase composition is the same as that of the amorphous phase constitution within the experimental error.

Small-Angle X-ray Investigations. The crystallinity of the copolymer samples was determined from the

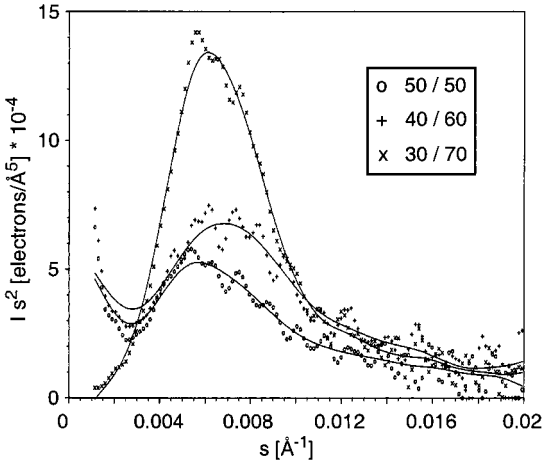

Figure 12. Lorenz-corrected small-angle X-ray pattern for PEBB/EN random copolymers.

Table 9. Results of DSC Measurements on PEBB/EN Copolymers[a]

EBB/EN	ω_c (%)	L (Å)	C (Å)	T_m (K)	ΔH_m (kJ/mol)
50/50	13	210	28	555	13.1
40/60	21	140	30	535	10.3
30/70	28	165	46	517	11.7

[a] For some copolymers, a broad transition with multiple maxima was measured during the second heating run.

invariant of small-angle X-ray patterns. The invariant is defined as

$$Q = \int Is^2 \, ds \tag{1}$$

where I is the s-dependent intensity and $s = 2(\sin\theta)/\lambda$; 2θ is the scattering angle and λ the wavelength of the X-rays. The crystallinity is calculated from the invariant as

$$Q = \omega_c(1 - \omega_c)(\Delta\eta)^2 \tag{2}$$

with $\Delta\eta$ being the electron density difference between the amorphous and the crystalline phase. $\eta_{amorphous}$ was estimated by linear extrapolation of the amorphous densities of the homopolymers and $\eta_{crystalline}$ from the PEN and PEBB crystal density using a parabolic function that was estimated from the abovementioned atomistic models. The lamellar thickness was calculated as $C = L\omega_c$, where L is the long period taken from the maximum of the Lorenz-corrected scattering data which are presented in Figure 12. The data are collected in Table 9.

It was found that the crystallinity increases with increasing concentration of the EN comonomer for the range of composition that was studied. This gives rise to the assumption that, in a range of EN concentration below 50%, the crystallinity of copolymers is very low. The lamellar thickness varies in the range of two or three constitutional repeat units and is thus much shorter than those estimated for PEN homopolymers.[22] PEBB homopolymers were not measured because the samples could not be prepared in the same way as the copolymers.

DSC Experiments. The melting temperatures of the copolymers decrease with increasing amount of EN comonomers in the copolymer. The lowest melting temperature can be observed between 70% and 80% EN, where the type of the crystal lattice changes to the PEN type. The crystal melt enthalpy, obtained by dividing the experimental melt enthalpy $\Delta H°_m$ (measured on the same samples that were used for small-angle X-ray scattering) by the crystallinity, is unexpectedly high for the samples with 50−70% EN concentration. However, the melt enthalpy can also contain contributions from a rigid amorphous phase[21] and it is thus difficult to analyze the results. In general, the melt enthalpy should be lower than that of the homopolymers, which is 25 kJ/mol for PEN.[21] For PEBB, no data can be found in the literature; we estimate $\Delta H°_m$ to be 28 kJ/mol by scaling the PEN result with the higher molar mass of PEBB.

From these results we come to the following conclusion: in the range of low EN concentration, which was not included in our investigation, nothing can be stated from our experiment, but the lower crystallinity of the copolymer containing 50% EN gives an indication that the EN comonomers are rejected from the crystals; i.e., only the EBB sequences are able to crystallize. In this case, the average length of EBB sequences drops and limits the size of the crystals. Hence, only a small amount of stable crystals are created. For copolymers with 50−70% EN, the increasing crystallinity can be explained assuming comonomer inclusion. The sequence length effect on crystallization vanishes and the crystallinity can be as high as for the homopolymer. However, the crystals are imperfect and the crystal melt enthalpy does not take into account this imperfection energy. For the 70% EN copolymer, where uniform inclusion is revealed by solid-state NMR experiments, the comonomer inclusion Gibbs energy ϵ is given by

$$T_m(X_{EN}) = T°_m\left[1 - \frac{\epsilon(X_{EN})X_{EN}}{\Delta H°_m} - \frac{\sigma_e}{\Delta H°_m C}\right] \tag{3}$$

$T°_m$ is the homopolymer equilibrium melting temperature (we used the Meurisse result of 623 K, see Table 1) and σ_e the lamellar surface free energy; since σ_e of PEBB is yet unknown, we use the experimental value of 0.06 J/m^2 obtained for PEN[22] as an estimate. Fitting the data from Table 9 to eq 3 reveals a defect inclusion Gibbs energy of 3.6 kJ/mol. This value is in the range of RT_c (T_c is the crystallization temperature), and thus consistent with the uniform inclusion model. Randomness of the guest-units position in the crystal is assumed by this model (the conformational entropy is neglected in eq 3) but not experimentally confirmed. We will address this question in the next chapter, where the defect inclusion Gibbs energy is estimated from computer simulations.

Free Energy Calculations

The purpose of this section is to investigate from the thermodynamic point of view the cocrystallization of random PEBB/EN copolymers by means of force-field computer simulations. We are considering different microstructures with specific comonomer arrangements or degrees of disorder. Our measure is the defect Gibbs energy of comonomer inclusion, ϵ, that is the Gibbs energy required to replace one monomer in a homopolymer crystal by a comonomer (Figure 13a).

As this direct exchange is difficult to model, we calculate ϵ in two independent calculations: the first is the transformation of a host−polymer repeat unit into a comonomer unit, and the second is the reverse transformation of a comonomer unit into a host−

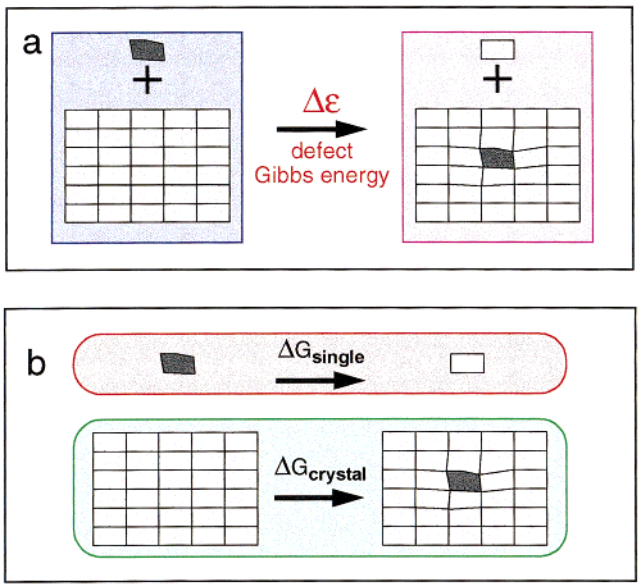

Figure 13. Concept of the defect inclusion procedure. Part a shows the direct exchange of one host−polymer repeat unit by one guest unit; this exchange requires the defect Gibbs energy ϵ. Part b shows the computational treatment of this exchange where the crystal and the single unit are transformed independently.

polymer unit; this second transformation is performed in a vacuum (Figure 13b). The sum of the two processes yields the desired quantity. The thermodynamic integration approach[12] was employed using the Discover molecular dynamics program[19] and the PCFF91 forcefield.[20]

Thermodynamic Integration. Thermodynamic integration is widely used for the prediction of the free energy changes accompanying chemical modifications.[5,23,24] In general, this method describes the transformation of a given system from an initial state $\lambda = 0$, characterized by the Hamiltonian H_0, to a new state $\lambda = 1$ (with Hamiltonian H_1) on a fictitious transformation path. The path is described by the transformation coordinate λ that runs from 0 to 1 and the related Hamiltonian H_λ is a combination of H_0 and H_1, i.e., $H_\lambda = f(1-\lambda)H_0 + f(\lambda)H_1$, where $f(\lambda)$ and $f(1-\lambda)$ can be any continuously differentiable function of λ.

From the thermodynamic point of view, the Helmholtz energy difference $\Delta A_{0\to1} = A_1 - A_0$ related to this transformation in an *NVT* ensemble is given by[24]

$$\Delta A_{0\to1} = \int_0^1 \left\langle \frac{\partial H(\lambda)}{\partial \lambda} \right\rangle_\lambda \mathrm{d}\lambda \qquad (4)$$

The Gibbs energy $\Delta G_{0\to1}$ is obtained by either performing the thermodynamic integration calculations in an *NpT* ensemble or by correcting $\Delta A_{0\to1}$ for the mechanical work energy $\langle p\rangle\Delta V$. A detailed description of the simulation procedure for the poly(ethylene terephthalate-*co*-naphthalene-2,6-dicarboxylate) (PET/EN) random copolymer is given elsewhere.[5,23] This procedure was adapted to the dicarboxy naphthanoate to bibenzoate transformation; here, we only report the details relating to this specific transformation. For all discussions, a value of $\lambda = 0$ is considered to be a EN structure, whereas a value of $\lambda = 1$ corresponds to the EBB structure.

Combined Repeat Unit. Figure 14 presents the model used for the transformation between EN and

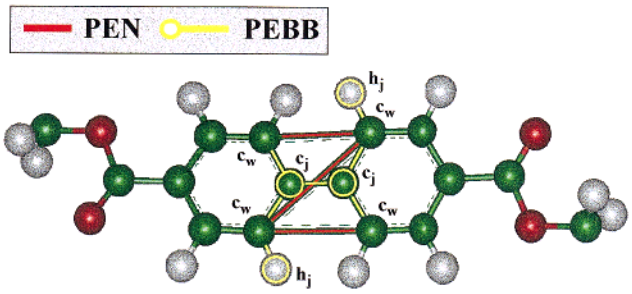

Figure 14. Combined naphthanoate−bibenzoate repeat unit. See text. The PEN repeat unit is obtained when the dark labeled bonds are switched on ($\lambda = 0$) while the PEBB repeat unit is obtained when the light labeled bonds and atoms are active ($\lambda = 1$).

EBB. It contains both "limiting structures" (i.e., EN and EBB) which are present during the transformation, each partial with respect to the actual value of λ. Notice that the EN repeating unit is obtained when the dark bonds are switched on ($\lambda = 0$) while the EBB repeating unit is obtained when the light bonds and atoms are active ($\lambda = 1$).

The letters in Figure 14 denote the atom types in the PCFF91 force field. "c_j" and "h_j" are used to describe the carbon and hydrogen atoms of aromatic molecules that need to be "created" during the transformation. Hence, the corresponding force field parameters were scaled. Atoms with atom type "c_w" were aromatic carbon atoms similar to "c_j" but present in both structures, so their force field parameters were not altered during the thermodynamic integration calculation, but it was necessary to rename these atoms to have the possibility of addressing bonds to other atoms that might be created.

Force Field Scaling. A scaling proportional to λ^2 is employed for all internal energy force constants k, giving a λ^2-dependent contribution of the internal potential energy to the Hamiltonian H. This scaling leads to an analytical derivative of

$$\frac{\mathrm{d}H(\lambda)}{\mathrm{d}\lambda} = 2\lambda H_{\text{internal}}^{\text{unscaled}} \qquad (5)$$

where $H_{\text{internal}}^{\text{unscaled}}$ denotes the unscaled energy expression used in the original force field. Similar to the PET−PEN transformation previously reported,[23] a scaling of some equilibrium bond lengths was employed to control the shape of the repeat unit during the transformation. The complete scaling functions are $1.3823 + 1.55\,\lambda$ for the c_w−c_w bond and $0.3823 + 4(\lambda - 0.5)^2$ for the c_j−c_j bond.

The nonbonded energy was scaled with the same λ^2 dependence, except for some intramolecular nonbonded interactions of atoms which are able to come very close to each other by the influence of the force-field scaling (e.g., all 1−4 van der Waals and Coulomb interactions, which are created or annihilated during the transformation). To prevent singularities in the molecular dynamics calculations, we applied a smoothing function for these nonbonded interactions.[23] All these interaction energies and gradients were calculated in a home-built program written in C that runs in parallel to the Discover MD program and communicates via the Discover interprocess communication (IPC) port.[19]

The Transformation in a Free Chain in Vacuum. The polymer chains in a PEBB or PEN crystal are

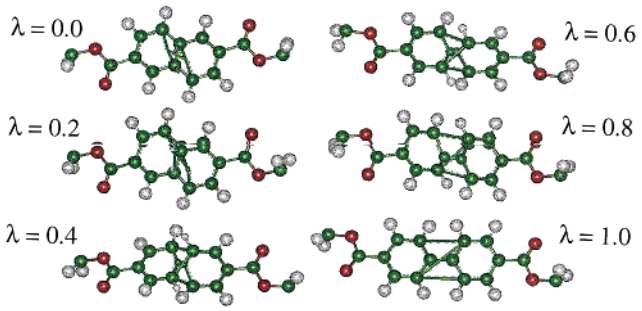

Figure 15. Snapshots of the repeat unit under transformation taken from molecular dynamics calculations on short polymer chains.

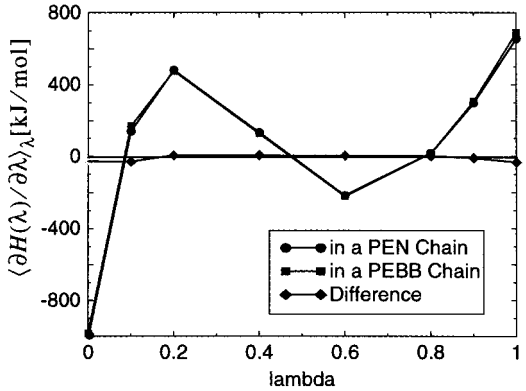

Figure 16. Graphical demonstration of the thermodynamic integration calculation on the transformation naphthanoate–bibenzoate in two independent calculations.

essentially in an "all-trans" conformation with deviations of the single torsions within a few degrees. Therefore, a suitable model for the reverse transformation is a short, extended single chain. We used a chain that contains only three repeat units, the central one of which was transformed. The applied nonbonded interaction-cutoff distance was shorter than the repeat unit length of any polyester under consideration; therefore, the results should not depend on the chemical structure of the aromatic unit of the first and third repeat unit, i.e., whether it is naphthalene or biphenylene. However, we performed two independent calculations with different chemical structures (both naphthalene or both biphenylene) for the first and third repeat unit in order to estimate the errors occurring in the thermodynamic integration procedure from two independent runs. The noncoiled conformation was preserved by constraining the end-to-end distance to between 25 and 45 Å with a flat bottomed potential. Figure 15 shows the shape of an arbitrary snapshot of the second repeat unit, that under transformation, for different values of λ. It is obvious that almost no deformation of the flat-shape character of the aromatic parts occur during the transformation, such a deformation being prevented by the scaling of several bond lengths.

The mean derivatives $\langle \partial H(\lambda)/\partial\lambda \rangle_\lambda$ plotted in Figure 16 are calculated from molecular dynamics runs of 500 ps for each value of λ. Snapshots were taken every 1 ps to calculate the derivative. The calculated derivatives are similar for both calculations, and the difference is in the range of the statistical deviations. The integration, applying the trapezoidal integration rule between the calculated λ points, gives 85 ± 10 kJ/mol for the transformation in a PEN chain segment and 88 ± 10 kJ/mol for the transformation in a PEBB chain segment. We define the mean value of 86 kJ/mol as the reference value of this type of transformation.

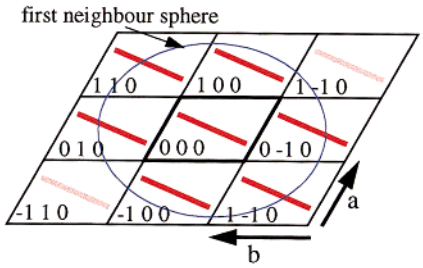

Figure 17. Schematic description of the first neighbor sphere in the $a-b$ plane around a test repeat unit at (000).

Table 10. Gibbs Free Energy (in kJ/mol per Defect) and Their Statistical Deviations for Single and Double Defect Inclusions, for Bibenzoate Units in a PEN Microstructure and for Naphthanoate Units in a PEBB Microstructure

type of inclusion	EBB in a PEN crystal	EN in a PEBB crystal
single defect at (000)	85 ± 18	55 ± 19
double inclusion at (000) and (100)	81 ± 26	56 ± 27
double inclusion at (000) and (010)	62 ± 26	49 ± 28
double inclusion at (000) and (110)	71 ± 26	54 ± 27

Defect Free Energy for Single and Double Defects. The computational setup to calculate the defect Gibbs energies of comonomers that are included into the host crystal is discussed elsewhere.[23] Following this scheme, we calculated the defect Gibbs energies for single comonomer inclusions and aggregates of comonomers that are juxtaposed spatially for all possible alignments inside the crystal $a-b$ plane. There are six neighboring sites inside the first neighbor "sphere", as shown in Figure 17, but they are symmetry-matched in three pairs. The calculated Gibbs energies for single and double comonomer inclusions are given in Table 10. The error values reported there are relatively high because of the large fluctuations of the derivatives $\partial H(\lambda)/\partial\lambda$ and the low number of conformations analyzed.

From these data, a simple trend can be observed: an aggregation of comonomers is preferred in the (010) and (110) directions but there is only a weak tendency toward aggregation in the (100) direction. This may be related to the polymer conformation as follows: the chain contour looks almost flat with only little structure in the directions perpendicular to the benzene or naphthalene rings (the (100) direction); therefore, they can easily slip over one another and a steric mismatch is not that important. However, the chains have a zigzag-type conformation in the (010) and (011) directions and are in register with the neighboring chains; therefore, stronger steric interactions occur. Then the aggregation of equal repeat units in these directions reduces the steric mismatch between them. Whereas aggregates of two defect units give defect free energies which are still too high to expect cocrystallization, larger aggregates, i.e., defects with a lower surface per volume, may be included into the crystal.

Although such larger aggregates can lower the total defect Gibbs energy, they do not in all cases reach a value in the range of RT_c (T_c: crystallization temperature) that enables cocrystallization from the thermodynamic point of view. When all six sites around a test comonomer unit at (000) are also seated with comonomers, the defect Gibbs energy related to the test

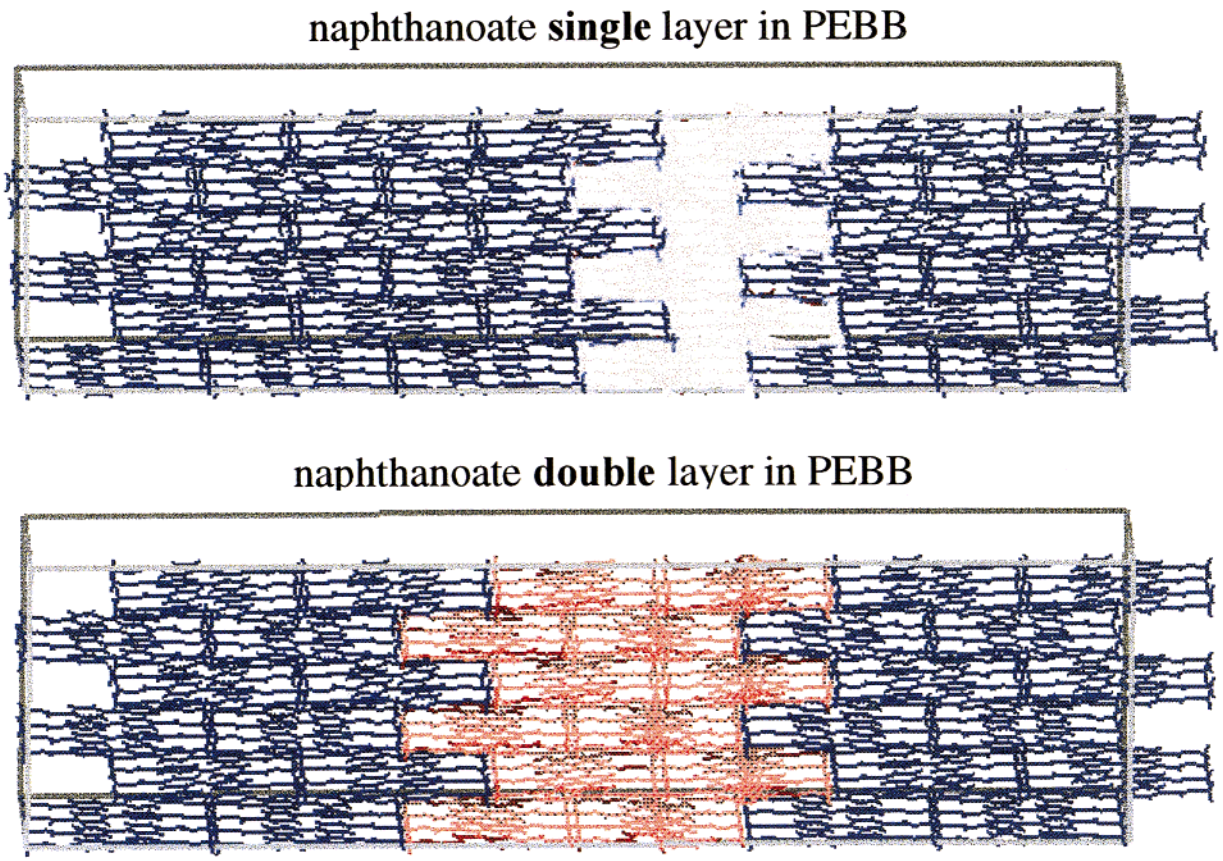

Figure 18. PEBB crystal including a single naphthanoate sheet and a naphthanoate double sheet. Different tricycles are used to indicate the units.

comonomer would reduce to 3 ± 48 kJ/mol for bibenzoate in a PEN crystal and to 43 ± 51 kJ/mol for dicarboxynaphthanoate in a PEBB crystal. These numbers are strongly dominated by statistical errors and can thus be much higher than RT_c, which is in the range of 4 kJ/mol. In addition, this approach neglects too many parameters, e.g., triple (and higher order) defect interactions and all interactions to other $a-b$ planes. Study of all possible interactions independently for sampling times long enough to obtain acceptable statistical errors far exceeds the available resources; therefore, we now focus on multiinclusions with selected comonomer concentrations and arrangements only.

Exchange of Sheets in the Crystal *a*−*b* Plane. This transformation can be performed by the thermodynamic integration technique within one single calculation. We focus on the transformation of EN into a PEBB crystal, which is most interesting from the experimental point of view. A single EN-type sheet and a EN-type double sheet (Figure 18) are investigated.

Thermodynamic integration calculations were performed in an NpT ensemble, thus allowing the periodic microstructure axes and angles to fluctuate. Figure 19 displays the average "cell" parameters as found in the simulated microstructure during the sampling for different values of the transformation path parameter λ. In the left half, the first sheet is transformed, and the second half describes the transformation of a second sheet directly adjacent to the first. Axes and angles vary between the values obtained at $\lambda = 0$ and $\lambda = 1$ with only minor fluctuations, thus indicating that the transformation runs on a continuous path. This is a necessary condition to obtain reliable thermodynamic integration results.

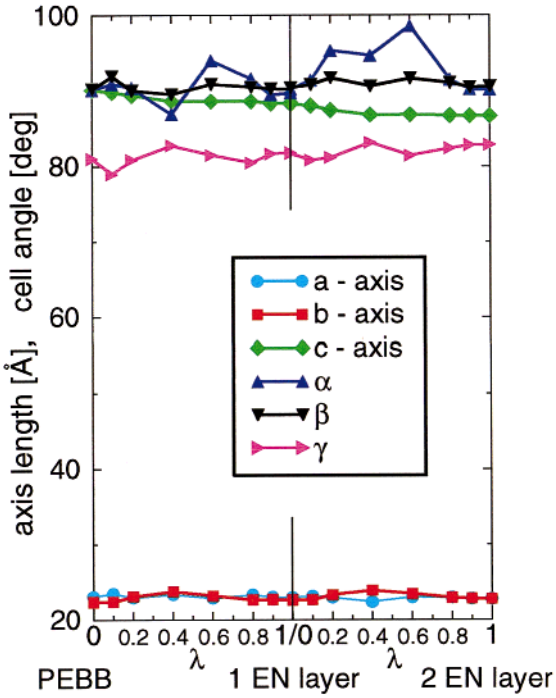

Figure 19. Fluctuation of the microstructure cell parameters during the modification of a bibenzoate sheet into naphthanoate (left) and the modification of a second sheet (right).

The results from thermodynamic integration calculations are 16 ± 6 kJ/mol per unit for the transformation of the first sheet. Comparing this result to 43 ± 51 kJ/mol calculated for the aggregates of double inclusions, a difference of 27 kJ/mol remains that is not captured

by the single and double inclusion approach. Although giving information on preferred alignments, the double inclusion approach cannot be used as an approximation for larger aggregates of repeat units in nonflexible copolymers, as the influence of an inclusion strongly extends to more than the nearest neighbor unit.

No additional defect Gibbs energy was found for the transformation of the second sheet; thus, the defect Gibbs energy is 8 ± 6 kJ/mol per unit for the double sheet (the statistical error did not change). Obviously, the dicarboxy naphthanoate repeat units within the $a-b$ sheet have already reached a minimum energy conformation that does not depend on the type of the next sheet, and the defect Gibbs energy is related to the surface energy between the EN layer and the PEBB crystal. Indeed, taking the Gibbs energy of 8 kJ/mol and the crystal unit cell dimensions reported in Table 4, the surface free energy is calculated to be 0.063 J/m^2, in good agreement to the value of 0.06 J/m^2 reported by Zachmann et al.[22] for lamellar PEN crystals.

Randomly Distributed Dicarboxynaphthanoate Inclusions. On the basis of single inclusion, double inclusion, and layer inclusion Gibbs energy results, a Hamiltonian to calculate the defect Gibbs energy of PEBB crystals containing randomly distributed dicarboxy naphthanoate comonomers was constructed. For each lattice site occupied by EN units, the total defect energy is 55 kJ/mol (single inclusion result). The total energy is then reduced by +1, +6, or −1 kJ/mol (depending on the orientation of the aggregates on the lattice) for all existing pairs of defects. For all existing triples of aggregated naphthanoate units, the total energy is further reduced 4.5 kJ/mol in order to obtain a total energy of 16 kJ/mol for a single layer type inclusion. This treatment is not straightforward (it is not suitable to fit the total defect Gibbs energy of random cocrystals), but it does force the formation of comonomer layers.

Crystals constituted by random comonomers (EN inclusions in PEBB crystals) were built and optimized according to the abovementioned Hamiltonian in a primitive lattice model already described in a former section of this paper ("calculation of copolymer crystal X-ray powder pattern"). An example on the effect of the optimization procedure is given in Figure 7. Whereas the initial structure appears completely random, EN-rich and EBB-rich layers are formed after optimization. From the model crystals with concentration 16.7%, 33.3%, and 50% EN, the one with the lowest potential energy was used for free energy calculations to estimate the defect inclusion Gibbs energy based on atomistic calculations.

The defect inclusion Gibbs energies were obtained to 35 ± 6 kJ/mol per defect for a nonoptimized 16.7% EN inclusion (one EN per stem), 25 ± 5 kJ/mol per defect for an optimized 33.3% EN inclusion (two EN per stem) and 10 ± 4 kJ/mol per defect for an optimized 50% EN inclusion. All multiple inclusion Gibbs energies for PEBB-based crystal structures are plotted in Figure 20.

After optimization, the parts of the EN units form an incomplete layer, thus reducing the average defect Gibbs energy. Other units remain more or less randomly arranged in the bibenzoate-rich region of the microstructure. Those regions have a higher defect Gibbs energy and might not crystallize in a real copolymer sample. The defect Gibbs energy of the naphthanoate-rich region would be necessarily lower and might reach values of 3.6 kJ/mol at an EN concentration of 70%, which we extrapolated from experiment (see above). This is also illustrated in Figure 20: the best estimate should be between the two lines that connect the results on layer type and random inclusions.

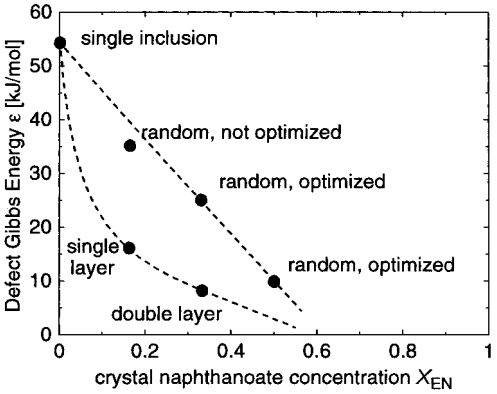

Figure 20. Defect Gibbs energy as obtained by lattice modeling (initial, random generated lattice, and optimized lattice) and defect Gibbs energies obtained by thermodynamic integration calculations.

Conclusion

This contribution deals with the nature of crystals of poly(ethylene-4,4′-biphenyldicarboxylate) (PEBB) and random copolymers of poly(ethylene-4,4′-biphenyldicarboxylate-*co*-2,6-naphthalenedicarboxylate) (PEBB/EN). Different polymorphs for the PEBB homopolymer were found, a suggestion for a second crystal unit cell, different from that which is discussed in the literature, was given by molecular modeling. A combined DSC, X-ray, and solid-state NMR analysis gave evidence that PEBB/EN random copolymers show uniform comonomer inclusion when the concentration of EN comonomers is high; for low EN concentrations, these comonomers are rejected from the crystals. By comparing the comonomer inclusion Gibbs energy, which was estimated from experiments, to those obtained from thermodynamic integration calculations, it was found that PEBB/EN copolymers are able to cocrystallize by aggregation of like and segregation of unlike repeat units. The short ethylene unit seems necessary to decouple the steric effect between the less flexible aromatic units along the polymer chains, thus reducing the influence of neighboring layers of different type on each other and allowing an optimized aggregation of the repeat units within one layer. Once these comonomer inclusions have reached a considerable size, the average defect Gibbs energy reduces to the thermal energy.

Acknowledgment. Important contributions came from L. Dirks (DSC), W. Gabrielse (solid state NMR), H. Goertz (X-ray), H. Linssen (liquid NMR), all DSM; A. J. J. Hendricks and J. Jager (synthesis), all Akzo Nobel; A. Kentgens and G. Nachtegaal from the University of Nijmegen (liquid NMR); and B. Nick (RWTH Aachen, computational discussions). We gratefully acknowledge support for J.W. from the Deutsche Forschungsgemeinschaft (Grant No. DFG We 2134/1-1).

References and Notes

(1) Flory, P. J. *Trans. Faraday Soc.* **1955**, *51*, 848.
(2) Baur, V. H. *Makromol. Chem.* **1966**, *98*, 297.
(3) Helfand, E.; Lauritzen, J. I. *Macromolecules* **1973**, *6*, 631.

(4) Sanchez, I. C.; Eby, R. K. *Macromolecules* **1975**, *8*, 638.
(5) Wendling, J.; Suter, U. W. *Macromol. Theory Simul.*, in press; *Chimia* **1998**, *52*, 607.
(6) Biswas, A.; Blackwell, J. *Macromolecules* **1988**, *21*, 3146 ff..
(7) Hanna, S.; Windle, A. H. *Polymer* **1988**, *29*, 207. Hanna, S.; Romo-Uribe, A.; Windle, A. H. *Nature* **1993**, *366*, 546.
(8) Lu, X.; Windle, A. H. *Polymer* **1995**, *36*, 451.
(9) Li, X.; Brisse, F. *Macromolecules* **1994**, *27*, 2276.
(10) Meurisse, P.; Noël, C.; Monnerie, L.; Fayolle, B. *Br. Polym. J.* **1981**, *13*, 55.
(11) Krigbaum, W. R.; Asarar, J.; Toriumi, H.; Ciferri, A.; Preston, J. *J. Polym. Sci., Polym. Lett. Ed.* **1982**, *20*, 109.
(12) Wendling, J.; Gusev, A. A.; Suter, U. W. *Macromolecules* **1998**, *31*, 2509.
(13) Mitrach, K.; Pospiech, D.; Häussler, L.; Voigt, D.; Jehnichen, D.; Rätzsch, M. *Polymer* **1993**, *34*, 2469.
(14) Qing, Y.; Jiasong, H. *Polym. Bull.* **1992**, *29*, 633.
(15) Wilson, A. J. C. *Mathematical Theory of X-ray Powder Diffraction*; Philips: Eindhoven, The Netherlands, 1963.
(16) Aerts, J. *Polym. Bull.* **1996**, *36*, 645.
(17) de Dauberny, R. P.; Bunn, C. W. *Proc. R. Soc. London* **1954**, *A226*, 531.
(18) Mencik, Z. *Chem. Prum.* **1967**, *42*, 78.
(19) InsightII and Discover 3.1. MSI Molecular Simulations: San Diego, CA, 1996.
(20) Hwang, M. J.; Stockfisch, T. P.; Hagler, A. T. *J. Am. Chem. Soc.* **1994**, *116*, 2515.
(21) Cheng, S. Z. D.; Wunderlich, B. *Macromolecules* **1988**, *21*, 789.
(22) Buchner, S.; Wiswe, D.; Zachmann, H. G. *Polymer* **1989**, *30*, 480.
(23) Wendling, J.; Suter, U. W. *Macromolecules* **1998**, *31*, 2516.
(24) van Gunsteren, W. F.; Beutler, T. C.; Fraternali, F.; King, P. M.; Mark, A. E.; Smith, P. E. In *Computer Simulations of Biomolecular Systems: Theoretical and Experimental Applications*; van Gunsteren, W. F., Weiner, P. K., Wilkinson, A. J., Eds.; ESCOM: Leiden, The Netherlands, 1993.

MA982013R